Mon. Not. R. Astron. Soc. **000**, 000–000 (0000) Printed 1 February 2008 (MN LATEX style file v1.4)

Strong gravitational lensing by multiple galaxies

Ole Möller[1,2] and A. W. Blain[3]
[1] *Cavendish Laboratory, Madingley Road, Cambridge, CB3 0HE, UK*
[2] *Kapteyn Institute, PO Box 800, 9700 AV Groningen, The Netherlands*
[3] *Institute of Astronomy, Madingley Road, Cambridge, CB3 0HA, UK*

1 February 2008

ABSTRACT
We discuss strong gravitational lensing by multiple objects along any line of sight. The probability for strong gravitational lensing by more than one lens is small, but a number of strong lens systems in which more than one separate lens contribute significantly to the lensing potential will be detected in the large sample of lens systems compiled with new instruments. Using multi-lens ray-tracing, we estimate the likelihood for gravitational lensing by two lenses at different redshifts and investigate typical image geometries and magnification cross sections. We find that, for a cosmology with $\Omega_{\rm M} = 0.3$ and $\Omega_\Lambda = 0.7$, about one in twenty lens systems consist of two lenses with merging caustics. Multiple lens systems differ from single lenses as the presence of a second lens in close proximity along the line of sight leads to a strongly asymmetric potential, which increases the multiple imaging cross section and significantly changes the image configuration. The external shear induced by a second nearby galaxy, group or cluster can significantly affect image positions even for more widely separated lens pairs. Both of these effects must be accounted for in lens modelling. We also show how the presence of aligned discs in the pair of lensing galaxies can lead to very large high-magnification cross sections. Lensing by more than one galaxy along the line of sight can lead to interesting image configurations. Such systems will be important in future, both for constraining lens models of individual systems and for statistical lensing.

Key words: methods: numerical – galaxies: fundamental parameters – galaxies: groups of galaxies – cosmology: theory – gravitational lensing

1 INTRODUCTION

Gravitational lensing by galaxies is usually modelled using a single lens. Observational results from the CLASS survey (Myers et al. 1995) suggest a probability $p_{\rm s}$ for gravitational lensing of a source at $z > 1$ of about 10^{-3}, comparing well with the theoretical prediction by Pei (1995). The probability that two galaxies both lie close enough to the line of sight to strongly lens a background galaxy might be expected to be roughly $p_{\rm s}^2 \sim 10^{-6}$ and so one might conclude that it is very unlikely for a source to be lensed strongly by two galaxies at different redshifts. However, even though the number of known lens systems to date is still relatively small – about 50 strong lens systems are known (Falco et al. 1999) – there is strong evidence that single lens models cannot explain the image geometries and magnification ratios in all cases. First, the observed image positions and magnifications in some systems, like the 'Cloverleaf', require either an unreasonable large mass for the lens or a substantial component of external shear (Kneib et al. 1998; Kneib, Cohen & Hjorth 2000; Soucail et al. 2000) in order to explain the details of the observed image geometry. In some cases, the lensing galaxy has been found to be part of a compact group of galaxies, and including the potential of the group greatly improves the lens model (Keeton & Kochanek 1997; Keeton, Kochanek & Seljak 1997; Kundić et al. 1997; Möller & Natarajan 2000). Second, it has been shown recently for two lens systems detected in the CLASS survey that the strong lensing potential is due to two galaxies at different redshifts, suggesting that double lens systems are not that uncommon (Koopmans et al. 1999; Koopmans & Fassnacht 1999).

In the next years, it is expected that using a new generation of instruments, lens surveys will increase the number of known lens systems by at least a factor of about 10 (Blain 1996; 2000). The large sample of strong lens systems should then contain a significant number of cases in which a background source is lensed by two foreground galaxies.

Gravitational lensing by multiple galaxies has been investigated before by Kochanek & Apostolakis (1988, KA98 here-

after) and Seitz & Schneider (1992). In KA98 the authors studied lensing by two lenses at the same and at different redshifts using a very similar ray-tracing routine to that used in this paper. However, due to the severe limits imposed by the computing power available at the time, their work was necessarily restricted to the study of only a very small fraction of the parameter space and did not include lens evolution. Multiple lensing has also been investigated in the context of microlensing, where the lenses are point masses (Lewis et al. 1993; Schneider, Ehlers & Falco 1992; Wambsganss, Witt & Schneider 1992). In a cosmological context, multiple lensing is naturally incorporated in simulations which combine ray-tracing methods with N-body simulations (Jain, Seljak & White 2000; Wambsganss, Cen & Ostriker 1998). However, due to the resolution limit of the N-body simulations, such work is concerned with the lensing effect of large-scale structure, on cluster and supercluster scales, and not with the strong lensing effect due to individual galaxies.

In this paper, we investigate the expected fraction of double galaxy lens systems and their statistical and characteristic properties. In section 2 we outline the ray-tracing method and the model of the evolving galaxy population used. In section 3 we show how double lens systems differ qualitatively from single lens systems in terms of both lensing cross sections and image configurations. In section 4 we estimate the probability of double lensing as a function of source redshift. In section 5 we look at the statistical image geometries, such as the ratio of quadruple:double images and discuss the expected distribution of the masses and redshifts of the lenses. We discuss some more elaborate multiple lens models qualitatively in section 6 and look at some observational issues in Section 7.

2 METHOD

2.1 Ray tracing

The method used in this paper is based upon the ray-tracing routines developed and described in Möller (1997) and Möller & Blain (1998, MB98 hereafter). The statistical work in this paper requires a large number of multi-plane ray-tracing calculations which made it necessary to modify the routines in two ways:

(i) the deflection angle is calculated in two planes at different redshifts using the full multi-lens equation (Schneider, Ehlers & Falco 1992). For two lenses, the lens equation becomes:

$$\vec{\beta} = \vec{\theta} - \vec{\alpha_{\rm A}}\frac{D_{\rm AS}}{D_{\rm OS}} - \vec{\alpha_{\rm B}}\frac{D_{\rm BS}}{D_{\rm OS}}, \tag{1}$$

where $\vec{\beta}$ is the source position, $\vec{\alpha_{\rm A}}$ is the deflection due to the near lens A, $\vec{\alpha_{\rm B}}$ is the deflection due to the far lens B and $D_{\rm AS}$, $D_{\rm BS}$ and $D_{\rm OS}$ are the angular diameter distances between source plane S and lens A, lens B and the observer respectively.

(ii) the code uses an adaptive grid to find all the images and determine the magnifications and shears on both the image and source planes. In order to generate the adaptive grid on the image plane, a coarse grid of triangles is first lensed and a coarse magnification map is obtained, as described in MB98. Each element on the coarse grid is then divided again into $N \times N$ sub-elements, where N is chosen to be proportional to the magnification: $N = 2 + (\mu - 1)/33$, for $\mu < 100$ and $N = 5$ otherwise. The resulting adaptive grid is then divided into triangles and lensed. The position of the resulting images are then found and the magnifications calculated in the usual way. If necessary the procedure can be repeated, but we found that a single iteration was sufficient for this application. This improves the efficiency and achievable resolution of the simulations by more than an order of magnitude. A different choice of $N(\mu)$ is possible, but we did not find a scaling that provides a significantly better performance than the one we used.

In this paper we mainly consider spherical pseudo-isothermal mass distributions (PIMD) as deflectors, but the routine can deal with any parametric spherical or elliptical lens profile.

2.2 The lens profiles

Since we are interested mainly in a qualitative investigation of double lensing involving two galaxy lenses we consider here only simple spherical mass distributions. Galaxy lenses are often modelled using a singular isothermal sphere (SIS). Such a model is, however, unphysical due to the infinite central surface mass density and total mass. Real galaxies are more realistically modelled using a pseudo-isothermal profile with a projected surface mass density of the form (Kneib et al. 1996, Natarajan & Kneib 1997):

$$\Sigma(R) = \frac{\Sigma_0 r_0}{1 - r_0/r_{\rm c}}\left(\frac{1}{\sqrt{r_0^2 + R^2}} - \frac{1}{\sqrt{r_{\rm c}^2 + R^2}}\right), \tag{2}$$

where we choose a small core radius $r_0 = 0.1\,$kpc and a cut off radius of $r_{\rm c} = 100\,$kpc. The total mass enclosed is then,

$$M_{\rm tot} = \lim_{r\to\infty} M(r) = 2\pi\Sigma_0 r_0 r_{\rm c}, \tag{3}$$

and the deflection angle at impact parameter R is

$$|\vec{\alpha}_{\rm A,B}| = \frac{4GM_{\rm tot}}{(r_{\rm c} - r_0)Rc^2}\left[\sqrt{r_0^2 + r^2} - \sqrt{r_{\rm c}^2 + r^2} + (r_{\rm c} - r_0)\right]. \tag{4}$$

For realistic, small core radii, $r_0 \sim 0.1\,$kpc, the lensing cross section does not differ significantly from that of a truncated singular isothermal profile. However, since a singularity in the mass profile reduces the number of images by one, the number of images and image geometries are different in a singular and non-singular model.

2.3 The lens population

In order to investigate the statistical properties of double lensing, we created a list of 5000 lens pairs along the line of sight to a given source at redshift $z_{\rm s}$. The sample is determined randomly, using a simple Monte–Carlo sampling method (Press et al. 1988) from a Press–Schechter distribution function (Press & Schechter 1974),

$$dN(M,z) = \frac{\rho}{\sqrt{\pi}}\frac{\gamma}{M^2}\left(\frac{M}{M^*}\right)^{\gamma/2}\exp\left[-\left(\frac{M}{M^*}\right)^{\gamma}\right]dM, \tag{5}$$

where ρ is the mean smoothed density of the universe, $\gamma = 1 + n/3$ relates to the initial power spectrum index n,

Table 1: Parameters used in simulations.

Parameter	Symbol	Value
Hubble parameter	h	0.5
Density parameter	$\Omega_{\rm M}$	0.3
Cosmological constant	Ω_Λ	0.7
Critical density	ρ	$2.37\Omega_{\rm M}\,h^2 \times 10^{11}\,{\rm M}_\odot{\rm Mpc}^{-3}$
Initial power-law index	n	1
Maximum lens mass	$M_{\rm max}$	$10^{13}\,{\rm M}_\odot$
Minimum lens mass	$M_{\rm min}$	$10^{10}\,{\rm M}_\odot$
Minimum lens redshift	$z_{\rm min}$	0
Maximum lens redshift	$z_{\rm max}$	10
Mass parameter	M^*	$3.6 \times 10^{12}\,{\rm M}_\odot$
Halo cut-off radius	$r_{\rm c}$	100 kpc
Core radius	r_0	0.1 kpc

where we choose $n = 1$, corresponding to a scale-invariant spectrum, and

$$M^*(z) = M_0^*(1+z)^{-2/\gamma} \quad (6)$$

is a characteristic bound mass at redshift z. We convert the mass from the Press–Schechter function into a velocity dispersion for the PIMD model of the lens assuming a cut-off radius for the lens mass distribution of $r_{\rm c} = 100\,$kpc. Thus, the conversion from mass M to velocity dispersion $\sigma_{\rm v} \sim \sqrt{GM/2r_{\rm c}}$. With this conversion an M^* galaxy has an approximate maximum velocity dispersion of $245\,{\rm km\,s^{-1}}$ if $M^* = 3.6 \times 10^{12}{\rm M}_\odot$ (Blain, Möller & Maller 1999). As shown in Fig.1 this cut-off radius is chosen so that the largest fraction of lenses will have a separation of $\approx 1''$ as is found in the CLASS survey (Helbig et al. 1999). For SIS lenses, and hence also, approximately, for PIMD lenses with small cores, the Einstein radius $R_{\rm E}$ increases with the velocity dispersion $\sigma_{\rm v}$ as $R_{\rm E} \propto \sigma_{\rm v}^2$. Note that there is a degeneracy between the choices of $r_{\rm c}$ and M^*; neither value is constrained significantly by observations. The particular values are chosen so that the value of M^* agrees with Blain et al. (1999).

(i) the mass of both lenses has to lie in a range $M_{\rm min} < M < M_{\rm max}$, where the values of $M_{\rm min}$ and $M_{\rm max}$ are chosen so that less than 2 per cent of the single lensing cross section is due to objects lying outside this range. As shown in Fig. 2, the fraction of lenses with masses less than $10^{13}{\rm M}_\odot$ for a value of $M^* = 3.6 \times 10^{12}{\rm M}_\odot$ and $z_{\rm s} = 2$ is greater than 99 per cent.

(ii) All lenses with an Einstein radius $R_E < 0.1''$ are excluded from the sample. As shown in Fig. 1, lenses with smaller Einstein radii contribute less than 2 per cent to the total lensing cross section.

Overall, the error on the calculated lensing cross section for double lenses that is introduced by these selections is less than 5 per cent.

2.4 Placement of lenses

We choose random pairs of galaxies from the Press–Schechter distribution function which are placed at uniformly random positions on the lens plane inside a $4'' \times 4''$ field. The magnifications and image configurations for each case are then obtained using the ray-tracing method. The parameters for the simulation are summarized in Table 1.

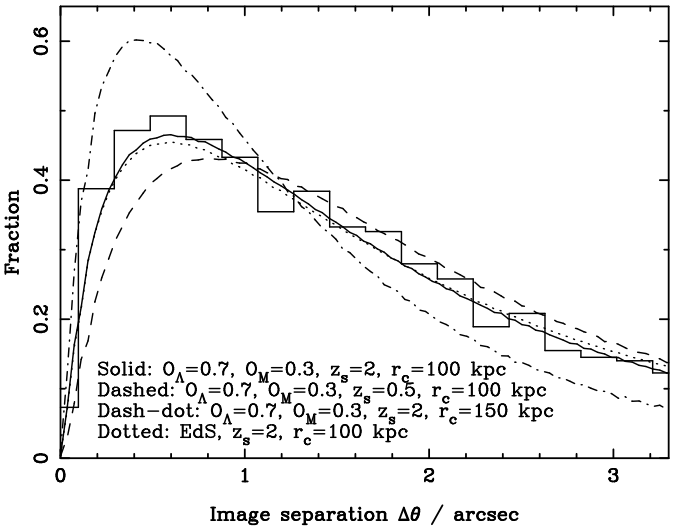

Figure 1. The contribution to the total cross section for lensing of sources at a single redshift $z_{\rm s}$ as a function of image separation. The solid curve is for sources at $z_{\rm s} = 2$ in a $\Omega_{\rm M} = 0.7$, $\Omega_\Lambda = 0.3$ cosmology and a lens populations with $M^* = 3.6 \times 10^{12}{\rm M}_\odot$, $r_0 = 0.1\,$kpc and $r_{\rm c} = 100\,$kpc. The histogram shows the total lensing cross section contribution toward $z_{\rm s} = 2$ in a sample of 10,000 lenses as used in the simulation. The dashed curve shows the expected distribution for the same lens population and cosmology but $z_{\rm s} = 0.5$. The dot-dash curve shows the expected distribution for a lens population with $r_{\rm c} = 150\,$kpc and the dotted curve is for an Einstein-de Sitter cosmology.

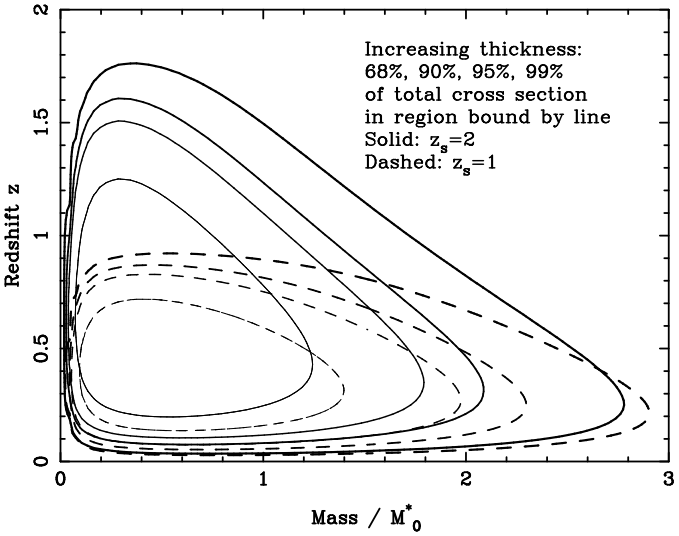

Figure 2. The contribution to the total lensing cross section of individual lenses as a function of the mass and redshift of the lens. The lens population is given by the Press–Schechter distribution function discussed in the text. The source redshift $z_{\rm s} = 2$ for the solid line and $z_{\rm s} = 1$ for the dashed line.

3 PROPERTIES OF INDIVIDUAL DOUBLE LENS SYSTEMS

3.1 Caustics and magnification of point sources

Two deflectors that are in close proximity to each other will modify their respective caustic structures in a way that de-

(a) (b)

Figure 3. Magnification maps and images for a double lens that consists of two PIMD halos with total mass of $M_{\rm tot} = 3 \times 10^1 2 {\rm M}_\odot$. The panel on the left shows the results on the source plane whereas the panel on the right shows the image plane. The lenses have redshifts $z_1 = 0.3$ and $z_2 = 0.6$ and the source plane is at $z_{\rm s} = 2.0$ In both panels the angular separation of the lenses is $\Delta\theta = 1.0''$ and they are placed equidistant from the origin. The grey-scale represents the total magnification of a source located at x, y in the source plane. The two white markers on panel (a) mark the positions of two point sources and the single contour represents the 0.5mJy contour of an extended source. In panel (b) the black markers show the image positions of the two point sources and the image of the extended source is shown as a grey scale. The large cross marks the position of the image(s) of the more distant lens. The thick, solid lines represent the caustics, in panel (a), and the critical lines, in panel (b). The dotted lines show the individual Einstein radii of the lenses.

(a) (b)

Figure 4. Magnification map on the source plane (a) and images (b) for double lenses, as in Fig. 3, but for $\Delta\theta = 2.0''$.

pends on their redshifts, mass profiles and separation. As a first step toward an understanding of double lensing, we used our routine to study the qualitative dependence of the magnification maps on the parameters of such systems.

Panel (b) of Figs. 3, 4, 5 & 6 show magnification maps and critical lines for two PIMD lenses at different redshifts for four different lens separations. The parameters for the figures are summarised in Table 2. These maps demonstrate four generic regimes that occur for double lenses. It is immediately apparent that the two lenses have a strong effect on each other – the magnification maps differ significantly from those of isolated spherical lenses. In particular, there are large high-magnification regions along the caustics. In Fig. 3 the two lenses are very close to each other and produce a joint caustic that is extended in a direction perpendicular to their separation. In Fig. 4 the lenses are further apart, but their individual Einstein radii still overlap. The caustic encloses a large area of high magnification in the source plane. In Fig. 5 the lenses are separated by more than the sum of their individual Einstein radii. In this geometry the caustic is extended primarily along the direction of the lens separation. In Fig. 6 the separation is sufficiently large that the Einstein radii do not overlap. However, there is still a 'trail' of high magnification between the two lenses in the source plane and there is sufficient shear to distort their individual caustics into astroids.

In Fig. 7 we show the cross section for magnification μ of point sources above a threshold value A for the four configurations of Figs. 3-6. Between magnifications of $\mu \approx 20$ and $\mu \approx 50$ there is an increase of up to a factor of ten as compared to the sum of the cross sections of individual lenses. The range of magnification for which there is a significant increase in the cross section depends on the degree of overlap between the Einstein radii of the lenses.

The results show qualitatively that double lens systems are much more likely to produce high magnifications of $\mu > 20$ for point sources as compared with isolated lenses. This discrepancy between the magnification distribution for double lens systems and the sum of the curves for the individual lenses demonstrates that magnification bias for double lens systems is expected to be large; hence the rough estimate of the double lensing probability as $\sim 10^{-6}$ given in the introduction is too small.

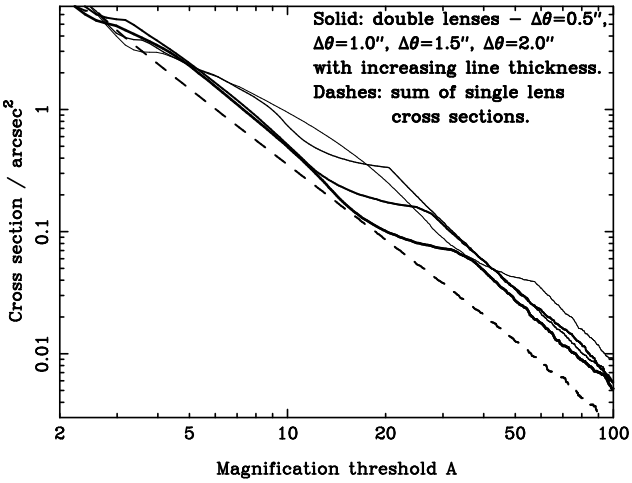

Figure 7. The lensing cross section for magnification of point sources above a threshold μ. The curves correspond to the four configurations shown in Figs. 3-6.

3.2 Image geometries

The images of point sources and one small, extended source are shown in panels (b) of Figs. 3-6 for the different source positions marked in the panel (a) to the left. In these panels, *all* images are shown, irrespective of their magnification. Those images which lie in the central region of the lenses will be strongly de-magnified and will, in most cases, not be observable. Discounting those images the panels show that, due to the extended shape of the caustics, four–image geometries are common. Point sources that lie in the high magnification region between the two lenses produce characteristic aligned triple images. Extended sources in the same region produce straight arcs with counterimages that lie on the opposite side of one of the lens centres.

In small–separation double lens systems with different redshifts the more distant lens can lie within the Einstein radius of the nearer lens, and so the more distant lens can itself be multiply imaged, leading to a total of six observed lensed images. The position of the images of the more distant lens is marked by a cross in panels (b) of Figs. 3-6. Also, for such small–separation systems, highly magnified sources are likely to have high image multiplicities, with three or five magnified images. For systems of intermediate separations,

(a) (b)

Figure 5. Magnification map on the source plane (a) and images (b) for double lenses, as in Fig. 3, but for $\Delta\theta = 3.0''$.

(a) (b)

Figure 6. Magnification map on the source plane (a) and images (b) for double lenses, as in Fig. 3, but for $\Delta\theta = 4.0''$.

as shown in Fig. 4, three magnified images may appear in a peculiar triangular configuration, with large and nearly equal separations between the three images. Systems with intermediate separations are also the most likely to produce triple aligned images or straight arcs, as in Fig. 5. Large separation double lens systems, as in Fig. 6, produce image configurations very similar to those of elliptical lens galaxies.

4 STATISTICS OF DOUBLE LENSED SYSTEMS

4.1 Definition of double lenses

In order to estimate the number of lens systems in which a background source is lensed by two foreground objects, it is first necessary to adopt a clear definition of what is meant by a "double lens". The number of systems in which a second galaxy introduces only external shear is certainly larger than the number of systems for which the background object would be multiply imaged by both lenses individually. Here we will define two regimes. A "weakly coupled double lens" is a lens system for which the caustics for each of the two lenses do not merge, but for which there is still a significant effect on the individual caustic structures. A "strongly coupled double lens" is a lens system in which the caustic structures merge. In other words, strongly coupled systems have a single connected multiple imaging region in the source plane, whereas weakly coupled systems do not. This distinction has the advantage that it is easy to classify objects in each regime from the topology of the inner caustic lines. A line connecting the two lenses will cross the high magnification caustic line less than twice only in the strongly coupled case. For example, the lens in Fig. 6 is a weakly coupled double lens, whereas that in Fig. 4 is a strongly coupled double lens.

4.2 Double lensing probability

The relative probability of double lensing is given by the cross section ratio of double lensing to lensing by the individual galaxies. The cross section due to double lensing is given by

$$\int_{\vec{\mathrm{p}}} \int_0^{z_s} \sigma(\vec{p}, z_s) n(\vec{p}) \frac{dV_{\mathrm{co}}}{dz}\, dz d\vec{p}, \tag{7}$$

where $\sigma(\vec{p})$ is the cross section for multiple images by a double system with parameters $\vec{p}$, $n(\vec{p})$ is the comoving number density of such systems and V_{co} is the comoving volume at redshift z. In our model the parameters of the system are the two redshifts, z_1 and z_2, the masses, m_1 and m_2, and the separation of the two lenses $\Delta\theta$. The comoving number density of objects

$$n(\vec{p}) = n(m_1, z_1) f(m_2, z_2, \Delta\theta), \tag{8}$$

where $f(m_2, z_2, \Delta\theta)$ is the probability of finding another lens with mass m_2 and redshift z_2 at a distance $\Delta\theta$. We assume no spatial correlation and so $f(m_2, z_2, \Delta\theta) = f(m_2, z_2) \times f(\Delta\theta)$. To proceed further it is necessary to compute the lensing cross section $\sigma(\vec{p}, z_s)$. Even though this is possible analytically in the case of simple lenses (KA98), the necessary formalism is cumbersome and cannot be extended to more elaborate lens models. Since the ray-tracing code described above is both extremely fast and accurate, we use it to obtain the form of $\sigma(\vec{p}, z_s)$ numerically. Instead of sampling the function $\sigma(\vec{p}, z_{\mathrm{s}})$ at regular intervals, to obtain an approximate functional form, we solve the complete integral in equation 5 numerically in a Monte–Carlo fashion. This is done by sampling lenses randomly from a Press–Schechter distribution as described in Section 2 and obtain the value of $\sigma(\vec{p}, z_s)$ for each lens system using ray tracing.

4.3 Numerical results

Using the lens population and ray tracing lensing routines described in Section 2, we obtain the expected number of double lens systems numerically for ten source redshifts in the range $0.5 < z_s < 10$. We calculate the total cross section for strong lensing by two lenses by summing the cross sections for multiple imaging calculated for each lens pair in our sample of 10,000 lenses for each source redshift, and then multiply this by the probability that two lenses with the given properties are found inside the $4'' \times 4''$ field. To obtain a conservative double lensing probability, we assume that there is no spatial correlation.

To test our procedure we also calculated the total multiple lensing cross sections due to the individual lenses. Fig. 8. shows the theoretical single lensing probability and the results from our simulations for the different source redshifts. As can be seen, the results agree well with the theoretical predictions. The errors are statistical and due to the finite number of lenses used – the numerical error introduced by the ray-tracing routine is several orders of magnitudes smaller.

Also shown in Fig. 8 is the probability of double lensing as a function of source redshift, for both weak and strongly coupled double lens systems. The dashed and dotted curves shown are obtained by squaring the probability for single lensing and normalising to the double lensing probability at $z_{\mathrm{s}} = 10$. Not surprisingly, the double lensing probability is consistently lower than that for single lenses. However, at redshifts larger than about 2 it is above the simple estimate from the introduction. This shows that the change in caustic structure due to the double lens potential cannot be neglected. Most noteworthy is that for source redshifts of about 5, about one in twenty lenses is expected to be a

Table 2: Parameters for lenses in Fig. 3-Fig. 6.

Parameter	Symbol	Fig. 3	Fig. 4	Fig. 5	Fig.6
Redshift lens A	$z_{\rm A}$	0.3	0.3	0.3	0.3
Redshift lens B	$z_{\rm B}$	0.6	0.6	0.6	0.6
Source redshift	$z_{\rm s}$	2	2	2	2
Lens separation	$\Delta\theta$	1"	2"	3"	4"
Position lens A	$\vec{\theta_{\rm A}}$	(0.35",0.35")	(0.71",0.71")	(1.06",1.06")	(1.41",1.41")
Position lens B	$\vec{\theta_{\rm B}}$	(-0.35",-0.35")	(-0.71",-0.71")	(-1.06",-1.06")	(-1.41",-1.41")
Core radius of lenses	r_0	0.1 kpc	0.1 kpc	0.1 kpc	0.1 kpc
Cut off radius of lenses	$r_{\rm C}$	100 kpc	100 kpc	100 kpc	100 kpc
Total lens mass	$M_{\rm tot}$	30 $M_\odot$	30 $M_\odot$	30 $M_\odot$	30 $M_\odot$

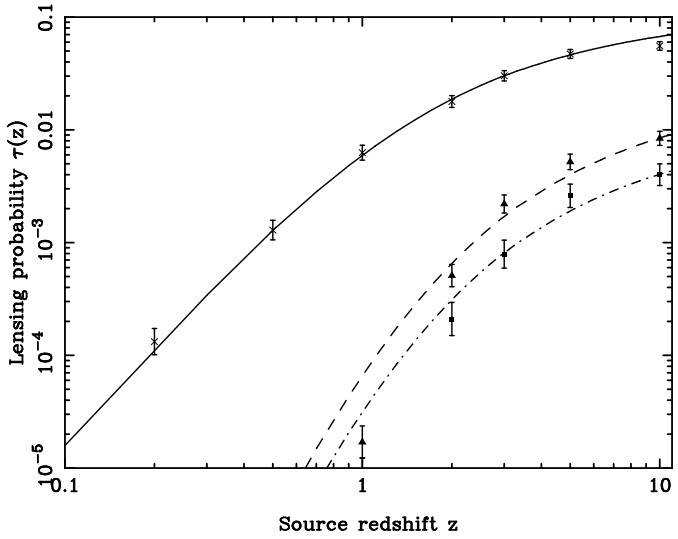

Figure 8. The probability of lensing for single and double lenses. The crosses show the results from our simulations as described in the text and the solid curve shows the analytical prediction for single lenses using SISs with a Press–Schechter distribution function. Squares show the probability for lensing by double lenses which have merging caustics ("strongly coupled double lenses"). Triangles show the probability for double lensing, including systems in which a second lens contributes significantly to the lensing potential ("weakly coupled double lenses"). The dashed and dot–dashed lines show the square of the single lensing probability normalised to the numerical results at $z_{\rm s} = 10$ for weak and strongly coupled double lenses respectively.

strongly coupled double lens. Also, the number of double lens systems at redshifts $z_{\rm s} \sim 1-2$ is in good qualitative agreement with the number of double lenses discovered so far in a radio–selected sample (two in a sample of 50).
We have not assumed any correlation in our lens sample. As the galaxy two-point correlation function is positive on these scales (Peebles 1993), our result is therefore likely to be an underestimate of the number of double lens systems in the case that the two lenses are at the same redshift. For a correlation of the form

$$\xi(r) = \left(\frac{r}{r_0}\right)^{-\alpha}, \qquad (9)$$

with $\alpha \approx 1.8$ and $r_0 = 5h^{-1}$Mpc at $z = 0$ we estimate that the two–point correlation increases the relative number of systems with separations below 1" by a factor of about 4. This means, that there will be an increase in the double lensing probability for correlated lenses at the same redshift relative to that for uncorrelated lenses of roughly the same factor. As shown in Fig. 7 double lenses are much more likely to produce high magnifications than individual lenses. Since flux limited lens surveys are biased towards the discovery of highly magnified images, the ratio of double lens systems to single lens systems in these surveys is likely to be higher than our prediction by a factor of a few.

5 STATISTICAL PROPERTIES

5.1 Lens properties

We have shown in the previous section that a large sample of gravitational lens systems is likely to contain a significant fraction of double lens systems. It is instructive to look at the properties of the double lens pairs in the sample.
Fig. 9 shows the contribution to the total lensing cross section as a function of the ratio of the two individual lens masses in panel (a) and as a function of the ratio of the two lens redshifts in panel (b). It can be seen that most of the double lens pairs in this sample have lenses lying at similar redshifts and with similar masses. This is not surprising, as the cross section for lensing of sources at a given redshift peaks at an optimal value of the redshift and mass of the lens galaxy. Positive spatial correlation will increase the number of double lens systems that are likely to lie at similar redshifts further. Note, however, that for uncorrelated pairs the efficency of lensing as a function of redshift is far less peaked for the second lens than that for a single lens (see, for example, Fig. 5 in Fukugita et al. 1992). In fact, the likelihood that the ratio of redshifts of uncorrelated double lenses is 2 or larger is ~ 50 per cent.

5.2 Statistical image geometries

Image geometries and magnification bias are strongly dependent on the mass profile of the lens, and so a two lens system is expected to lead to unusual and complex image geometries. In Section 2, we showed some individual image geometries for extended sources. To determine the statistical properties of the images, we generated images for small sources in the double lenses in our sample. The histogram of the cross section for the number of images is shown in Fig. 10. We show the results for two different sets of observational selection criteria. In panel (a) the statistics include all images, in panel (b) only images with minimum separation of $0.05''$ and a maximum magnification ratio of 100 are included and

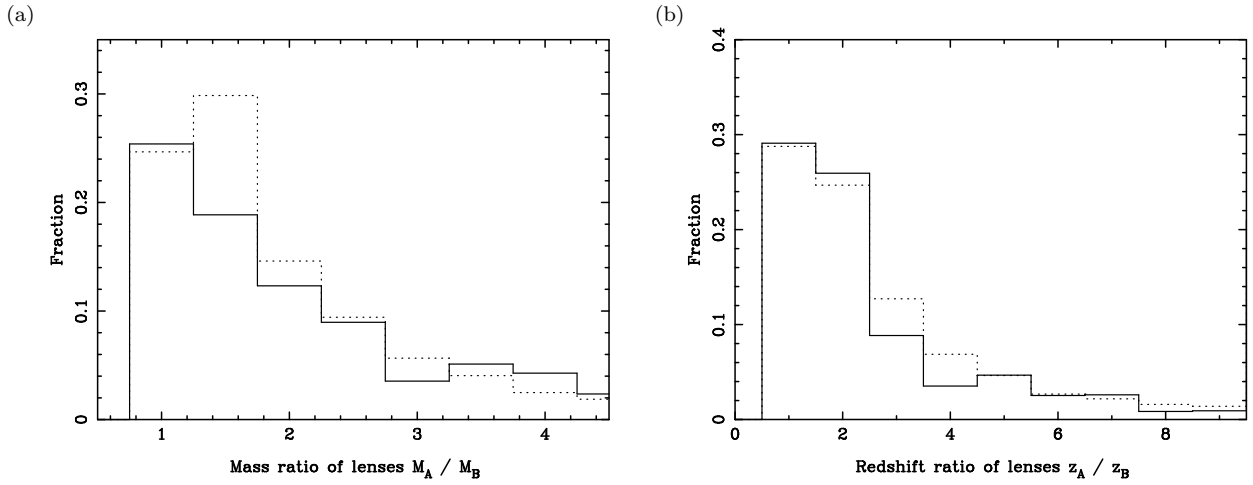

Figure 9. Properties of double lenses from a sample of 5000 pairs, generated as described in the text. The left panel shows the total lensing cross section by double lenses as a function of the mass ratio. The right panel shows the total lensing cross section as a function of the redshift ratio. The solid line represents lens systems in which the caustics of the two lenses merge ("strongly coupled double lenses"). The dotted line represents lens systems in which the caustics do not merge but in which the second lens produces significant external shear ("weakly coupled double lenses"). The source redshift is $z_s = 2$.

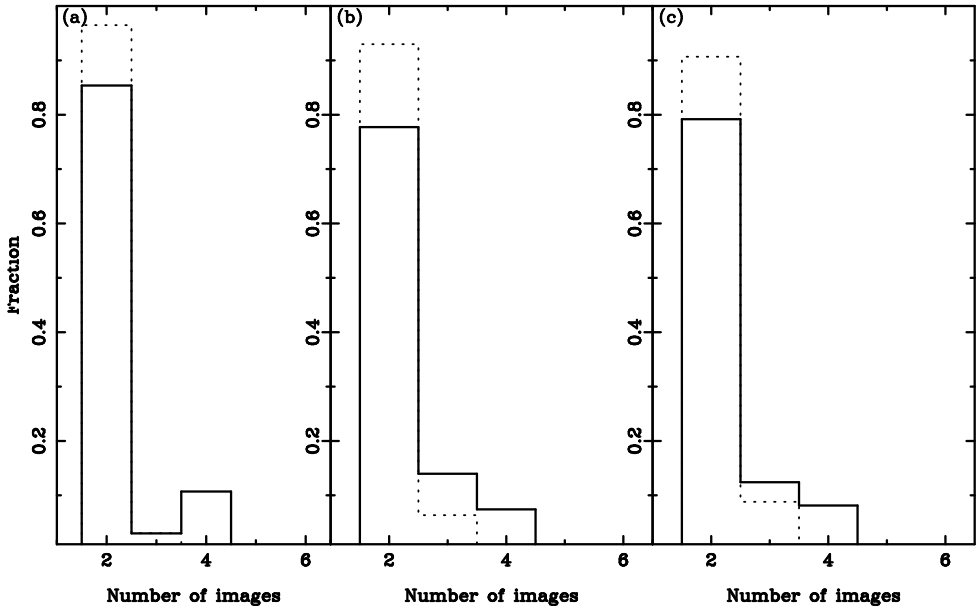

Figure 10. Number of images for strong and weakly coupled double lens systems. The solid line marks the histogram for strongly coupled double lenses in which the caustics merge. The dotted line marks the histogram for weakly coupled double lens systems in which a second lens introduces significant external shear but for which the caustics do not merge. The statistical uncertainty on all results shown in this figure is about 5 per cent. The source redshift is $z_s = 2$.

in panel (c) only images with minimum separation of $0.05''$ and maximum magnification ratio of 20 are included. The histograms show clearly the increased cross section towards three ($\sim 15\%$) and four ($\sim 10\%$) images. Individual spherical PIMD lenses can only produce two magnified and one demagnified image. Strongly coupled double lens systems can produce three or more magnified images. Strongly and weakly coupled double lenses both lead to quadruple systems and to a small fraction of five- and six-image systems. However, since the fraction of double lens systems will be small, and the vast majority of all lens galaxies are expected to have some effective elliptical profile, which increases the cross section for the formation of four or more images in a similar way, the effect of double lenses on the overall image statistics in a large sample of lenses will be small. Note that the image configuration shown in Fig. 5(b) is characteristic of double lens systems and hard to reproduce in most single lens models. Also, three strongly magnified images, without an additional counter-image, is a clear sign of a possible double lens system. Magnification bias in any flux limited lens sample will increase the relative number of lens systems with high image magnifications and hence high image multiplicities. This effect will increase the fraction of systems with 3 or more images by a few per cent.

6 EXTENDING DOUBLE LENS MODELS

6.1 Double lens plus external shear

Our above analysis does not assume any correlation between the lens positions, however, the spatial positions of galaxies on the sky are in reality correlated, and most galaxies occur in small groups or clusters. To show qualitatively how other galaxies in the environment affect double lensing, we model the potential perturbation due to a nearby group or cluster as an external shear that acts on the double lens system. In Fig. 11 we show the magnification maps for the double lens system shown in Fig. 5, now modified by an external shear, which is assumed to be perpendicular to the alignment of the lenses in Fig. 11(a) and parallel to the alignment of the lenses in Fig. 11(b). We model the source of the external shear as a point mass of $7 \times 10^{12}\,\mathrm{M}_{\odot}$ at a distance of 14 arcsec. In Fig. 11(a) the external shear "bends" the caustic structures in its direction, but the effect on the caustic area is small. It is only when the external perturber lies close to and is nearly perfectly aligned with the lens pair, as in Fig. 11(c), that the size of the caustic is affected significantly. Such a situation is likely to be rare, however, and so we expect that, on average, the effect on lensing statistics due to external shear from perturbers is likely to be small. However image positions and magnifications can be affected greatly by even moderate external shear, and so external perturbers have to be taken into account in accurate lens modelling of individual double lens systems. A more detailed treatment of the effect of external perturbers like groups of galaxies on the properties of galaxy lenses can be found in Keeton, Kochanek & Seljak (1997) and Möller, Natarajan & Kneib (in preparation).

6.2 Spiral galaxies

In the above analysis we kept the number of parameters as small as possible and used the PIMD as a simple but reasonable lens model. Including spiral discs into the lens model significantly changes the lensing behaviour of individual systems, as shown by Maller, Flores & Primack (1997) and MB98. The statistical lensing properties of spiral lenses has been investigated by Bartelmann & Loeb (1998), Keeton & Kochanek (1998) and Blain, Möller & Maller (1999). These studies showed that there is a significant effect on the properties of lensing by a single galaxy. We show qualitatively how the presence of spiral discs will affect double lensing in Fig. 12. Both lenses are spiral galaxies similar to the Milky Way, which consists of an PIMD halo and an inclined thin exponential disc, of central surface mass density Σ_0 and scale length r_{s}, containing about 10 per cent of the halo mass. The effect of the discs on the lens properties depends strongly on the relative alignment of the discs. If they are perpendicular to one another, then the shear along the caustics is greatly reduced and the area enclosed by the caustics shrinks drastically. If both discs are aligned with each other and the angle between their major axes is less than about 60 deg, then the caustic lines can enclose a very large high–magnification area as seen in Fig. 12(a). It is difficult to assess the effect of spirals on double lens systems in a statistical sense due to the large parameter space. The effect of discs on double lens statistics is expected to be small if the alignment of the discs is uncorrelated, as the asymmetry that is introduced in the potential by the disc will *on average* counteract the ellipticity introduced due to a second lens. Individual double spiral galaxy lenses will in general have different properties than double spherical or elliptical lenses. Spiral galaxies are at least twice as abundant as elliptical galaxies and therefore, since the inclination effect due to the discs enhances the high magnification cross section, double lens systems containing one or two spiral galaxies are likely. Observations of such lens systems could provide strong constraints on the mass profile of one or both lenses.

7 OBSERVATIONS OF DOUBLE LENSES

The observed properties of double lenses are likely to depend more strongly on the wavelength of observation than those of single lenses. This is due to the fact that light from the images and the more distant lens (or its images if it is multiply lensed by the nearer lens) is likely to be superimposed on the light distribution of the near lens galaxy. In addition, dust in the interstellar medium of the lens galaxies could lead to significant extinction of one or more of the images. Double lens systems will only be easily observable if both lenses are relatively faint at the wavelength of observation. This would be the case, for example, in the radio or sub-mm waveband if the two lenses are elliptical galaxies and the background source is a small young star forming galaxy. It would not be the case for optical observations of two massive spiral galaxies lensing a distant galaxy. In this case images are likely to be too faint relative to the lenses to be observable at most wavelengths. As quasar radio surveys are not affected by extinction, a complete lens sample from a radio survey, like the CLASS survey, would therefore be especially suited to observe double lens systems. The *Planck* mission will discover many thousands distant sources serendipitously at sub-mm wavelengths of which a fraction of order 10 per cent could be lensed (Blain 1998a). We predict that about 5 per cent of these lens systems will be double lenses. The Atacama Large Millimetre Array (ALMA) which will observe at sub-mm wavelengths would be well suited to detect the images of distant sources (Blain 1998b;2000). The subarcsecond resolution of ALMA would resolve the individual images and allow their direct study, which would greatly improve the accuracy of lens mass models.

8 CONCLUSIONS

In this paper we have investigated gravitational lensing of high-redshift background sources by more than one galaxy along the line of sight. Using a Press–Schechter halo distribution and a ray-tracing code we have estimated the number of double lens systems that are to be expected in a large lens sample. We have discussed the properties of such double lens systems and investigated more complicated double lens models qualitatively. In summary, our main results are:

(i) In a cosmology with $\Omega_{\Lambda} = 0.7$ and $\Omega_{\mathrm{M}} = 0.3$, about 2-5 per cent of all multiply imaged sources at $z \approx 2$ or higher are expected to be lensed by more than one lens along the line of sight.

(a) (b)

(c) (d)

Figure 11. Magnification maps and images for double lenses similar to those in Figs. 3-6 with an additional component of external shear. The lenses have the same parameters as those in Fig. 5 and are at $z_{\rm A} = 0.6$ and $z_{\rm B} = 0.3$ respectively with an angular separation of $3.0''$. Panels (a) and (c) show the source plane, panels (b) and (d) the image plane. The shear is due to an external point lens of mass $7 \times 10^{12} {\rm M}_{\odot}$ at a distance of $14''$at a redshift of 0.2. The mass lies in the lower left along the line connecting the lenses in the lower panels and in the bottom right along a line perpendicular to that connecting the two lenses in the upper panels.

(a) (b)

(c) (d)

Figure 12. Magnification maps and images for spiral double lenses. Panels (a) and (c) show the source plane, panels (b) and (d) the image plane. The lenses are both modelled as the sum of a PIMD and an exponential disc. The lens separation and PIMD halo properties are as in Fig.5. The discs have a surface mass density of $\Sigma_0 = 10^{10} {\rm M}_{\odot} {\rm kpc}^{-2}$ and a scale length of $r_{\rm s} = 3\,{\rm kpc}$. The lens in the top right of each panel is inclined at 75 deg towards the line of sight and is at $z_1 = 0.6$, whereas the lens in the bottom left of each panel is inclined at 65 deg to the line of sight at $z_2 = 0.3$. In the upper panels, the discs are aligned towards each other, in the lower panels they are aligned at right angles to the line connecting the two lenses.

(ii) The second lens induces a strong asymmetry in the effective lensing potential. This leads to a significant change in the caustic structure. The cross section for high magnification of point sources increases significantly due to this effect.

(iii) Double lenses lead to a significant fraction of lens systems with three ($\sim 15\%$) and four ($\sim 10\%$) images, and can lead to five- and six-image configurations.

(iv) The two lenses in a double lens system are likely to be of similar mass and redshift.

(v) Additional external shear acting on a lens pair can modify the caustic structure and the image geometries in individual systems significantly, and needs to be included in lens modelling just as for single lens systems.

(vi) Double spiral galaxy lenses can have a large high-magnification cross section, if their postion angles are aligned with each other, and the inclination of both of the discs towards the line of sight is higher than about 65 deg.

(vii) Future lens surveys, especially in the submillimetre wavebands will contain a significant number of double lens systems.

ACKNOWLEDGEMENTS

OM acknowledges the Lensnet TMR network and AWB the Raymond and Beverly Sackler Foundation for support. We thank Priya Natarajan, Daniel Mortlock and the referee, Jean-Paul Kneib for useful comments on the manuscript.

REFERENCES

Bartlemann M., Loeb A., 1998, ApJ, 503, 48
Blain A. W., 1996, MNRAS, 283, 1340
Blain A. W., 1998a, MNRAS, 295, 92
Blain A. W., 1998b, MNRAS, 297, 511
Blain A. W., 2000, in Wootten A., ed., Science with the Atacama Large Millimeter Array, PASP conf series, in press (astro-ph/9911449)
Blain A. W., Möller, O., Maller, A. H. 1999, MNRAS, 303, 423
Falco E. E., et al.,2000, in Brainerd T. & Kochanek C. S., eds., Gravitational Lensing: Recent Progress and Future Goals, ASP, San Francisco, in press (astro-ph/9910025)
Helbig P., Marlow D. R. Quast R., Wilkinson P. N., Browne I. W. A., Koopmans L. V. E. 1999, A&A Supp, 136, 297
Jain B., Seljak U., White S., 2000, ApJ, 530, 547
Keeton C. R., Kochanek C. S., 1997, ApJ, 487, 42
Keeton C. R., Kochanek C. S., 1998, ApJ, 495, 157
Keeton C. R., Kochanek C. S., Seljak U., 1997, ApJ, 482, 604
Kneib J.-P., Alloin D., Mellier Y., Guilloteau S., Barvainis R., Antonucci R., 1998, A&A, 329, 827
Kneib J.-P., Cohen J. G., Hjorth J., 2000, ApJL, submitted (astro-ph/0006106)
Kneib J.-P., Ellis R. S., Smail I., Couch W. J., Sharples R. M., 1996, ApJ, 471, 643
Kochanek C. S., Apostolakis J., 1988, MNRAS, 235, 1073
Koopmans L. V. E., et al., 1999, MNRAS, 303, 727
Koopmans L. V. E., de Bruyn A. G., Jackson N., 1998, MNRAS, 295, 534
Koopmans L. V. E., Fassnacht C. D., 1999, ApJ, 527, 513
Kundić T., et al., 1997, AJ, 114, 2276
Lewis G. F., Miralda-Escude J., Richardson D. C., Wambsganss J., 1993, MNRAS, 261, 647
Maller A. H., Flores R. A., Primack J. R., 1997, ApJ, 486, 681
Möller O., 1997, MSci Dissertation, Cambridge University
Möller O., Blain A. W., 1998, MNRAS 299, 845
Möller O., Natarajan P., 2000, in Brainerd T., Kochanek C. S., eds., Gravitational Lensing: Recent Progress and Future Goals, ASP, San Francisco , in press (astro-ph/9909303).
Myers S. T. et al., 1995, ApJ, 447, L5
Natarajan P., Kneib J.-P., 1997, MNRAS, 287, 833
Peebles P. J. E., 1993, Principles of Physical Cosmology, Princeton University Press, Princeton, p.213
Pei Y. C., 1995, ApJ, 440, 485
Press W. H. Flannery B. P., Teukolsky S. A., Vetterling W. T., 1988, Numerical Methods in C, Cambridge University Press
Press W. H., Schechter P., 1974, ApJ, 187, 425
Seitz S., Schneider P., 1992, A&A, 265, 1
Schneider P., Ehlers J., Falco E. E., 1992, Gravitational Lenses, Springer, New York
Soucail G., Kneib J.-P., Jansen A. O., Hjorth J., Hattori M., Yamada T., 2000, A&A, submitted (asto-ph/006382)
Wambsganss J., Cen R., Ostriker J. P., 1998, ApJ, 494, 29
Wambsganss J., Witt H. J., Schneider P., 1992, A&A, 258, 591


This figure "figure3a.jpg" is available in "jpg" format from:
http://arXiv.org/ps/astro-ph/0103093v2

This figure "figure3b.jpg" is available in "jpg" format from:

http://arXiv.org/ps/astro-ph/0103093v2

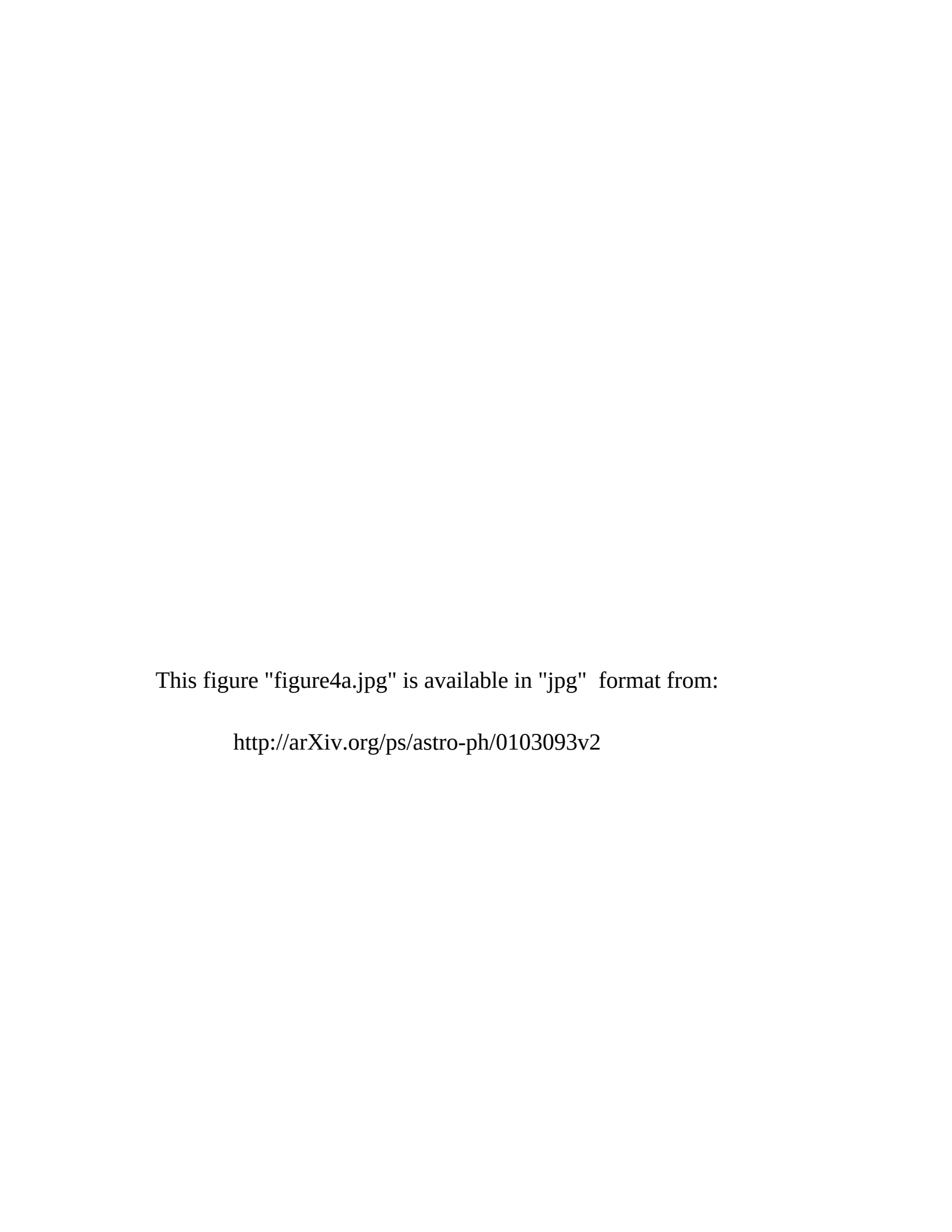
This figure "figure4a.jpg" is available in "jpg" format from:
http://arXiv.org/ps/astro-ph/0103093v2

This figure "figure4b.jpg" is available in "jpg" format from:

http://arXiv.org/ps/astro-ph/0103093v2

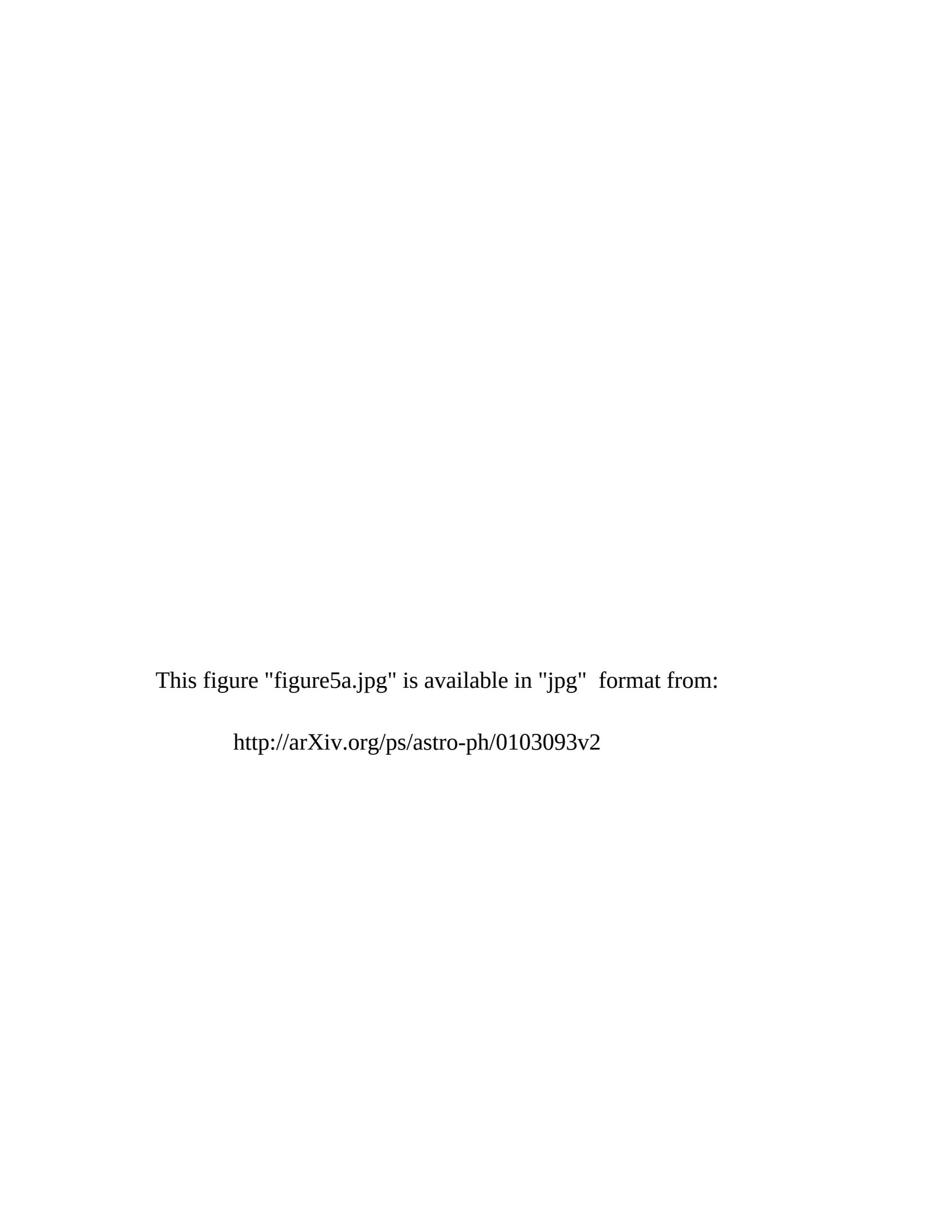
This figure "figure5a.jpg" is available in "jpg" format from:
http://arXiv.org/ps/astro-ph/0103093v2

This figure "figure5b.jpg" is available in "jpg" format from:

http://arXiv.org/ps/astro-ph/0103093v2

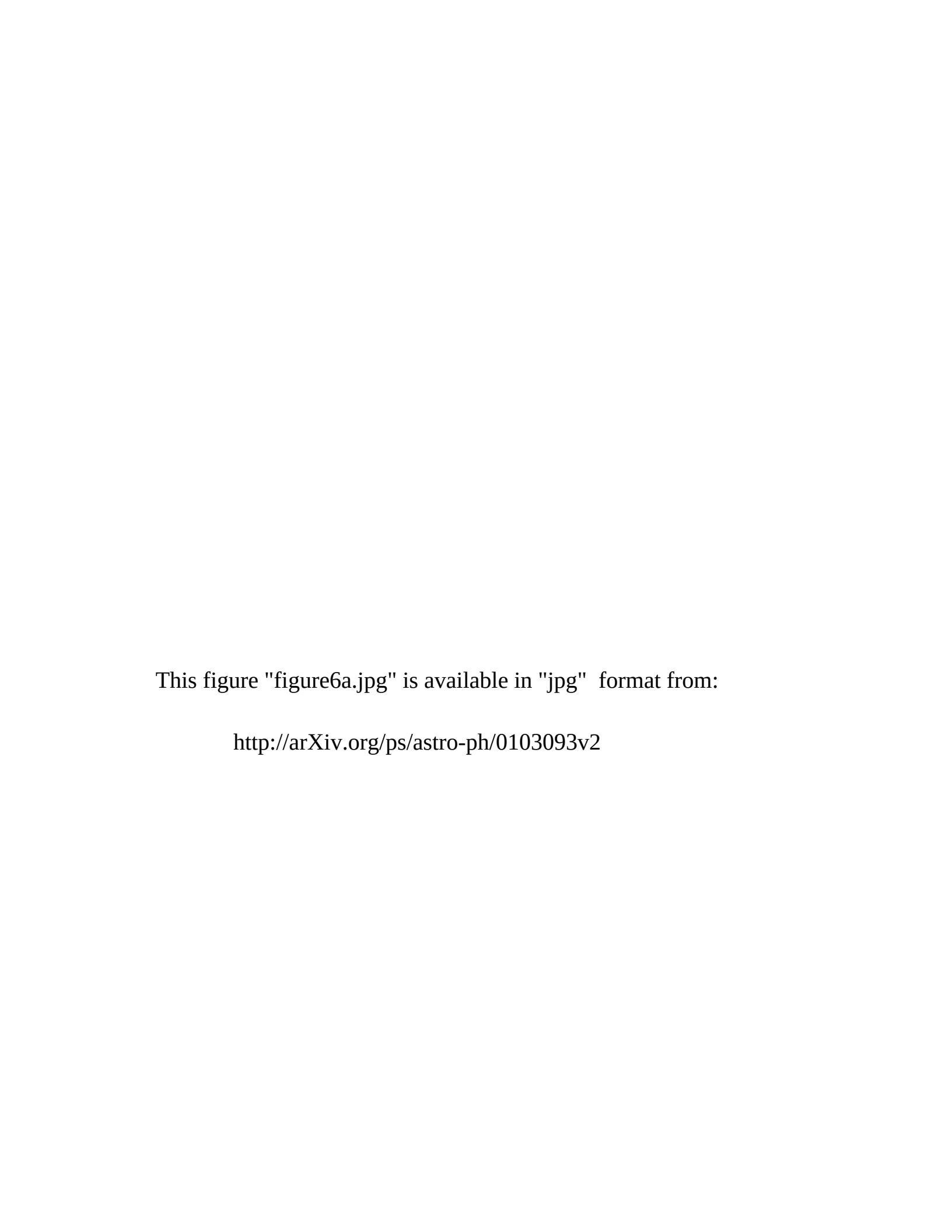
This figure "figure6a.jpg" is available in "jpg" format from:
http://arXiv.org/ps/astro-ph/0103093v2

This figure "figure6b.jpg" is available in "jpg" format from:

http://arXiv.org/ps/astro-ph/0103093v2

This figure "figure11a.jpg" is available in "jpg" format from:

http://arXiv.org/ps/astro-ph/0103093v2

This figure "figure11b.jpg" is available in "jpg" format from:

http://arXiv.org/ps/astro-ph/0103093v2

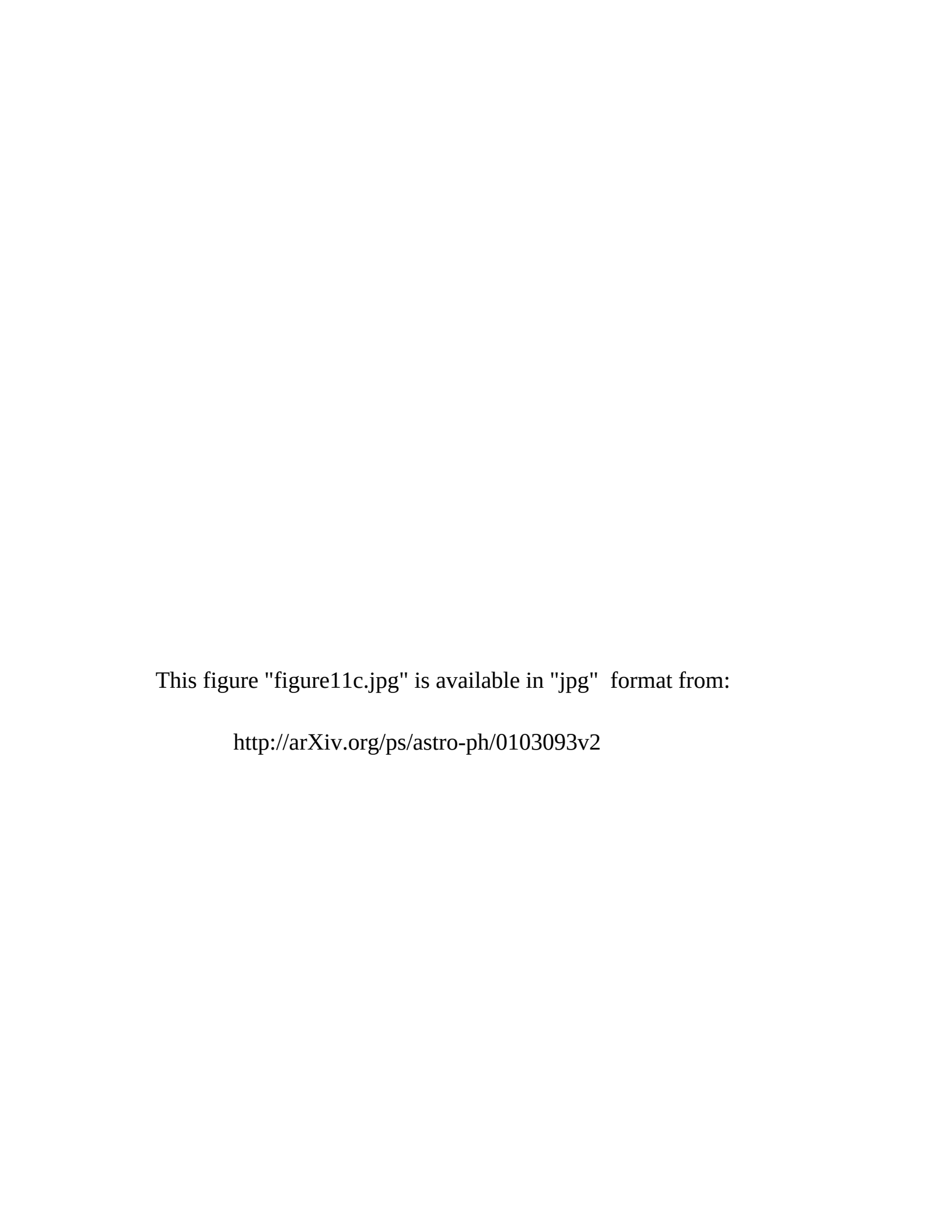
This figure "figure11c.jpg" is available in "jpg" format from:
http://arXiv.org/ps/astro-ph/0103093v2

This figure "figure11d.jpg" is available in "jpg" format from:

http://arXiv.org/ps/astro-ph/0103093v2

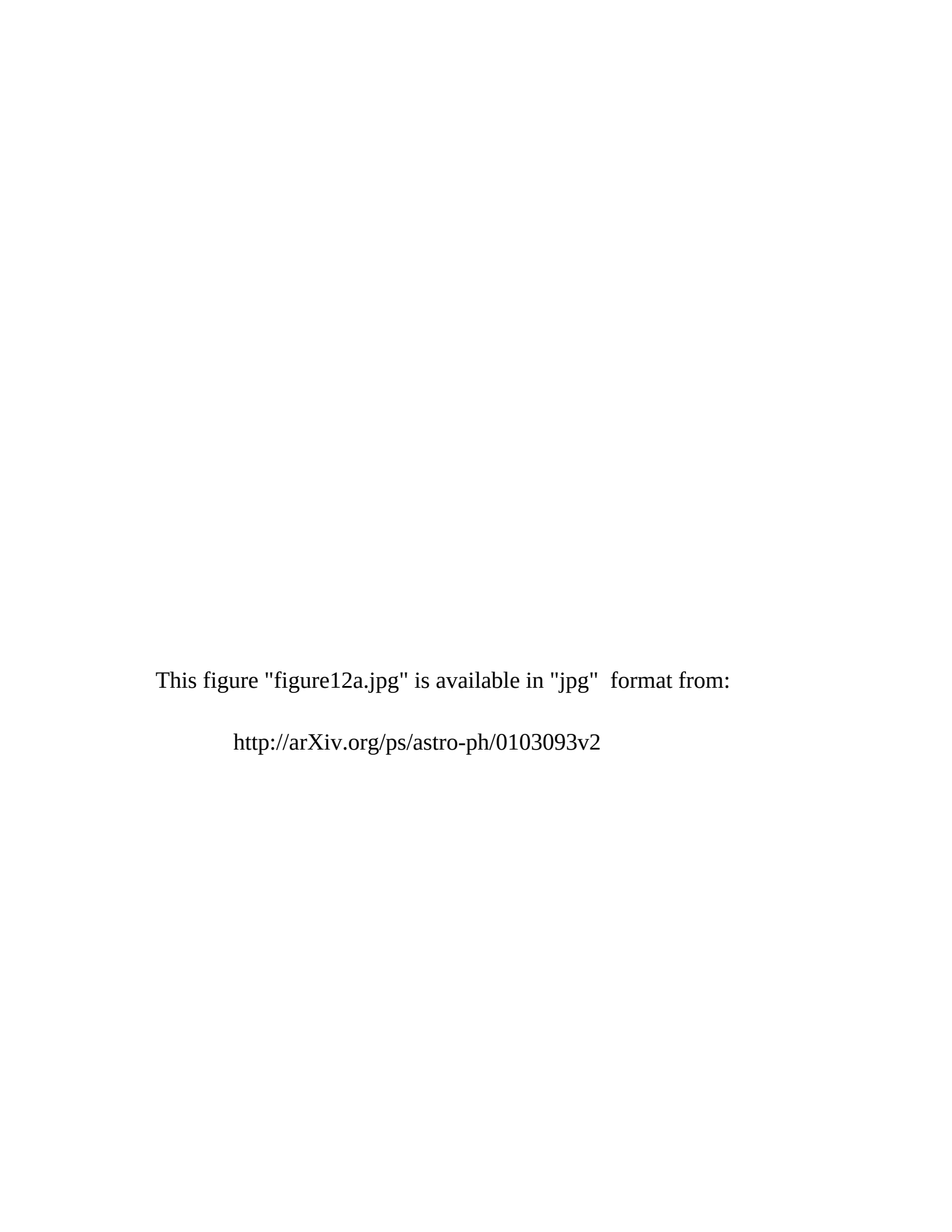
This figure "figure12a.jpg" is available in "jpg" format from:
http://arXiv.org/ps/astro-ph/0103093v2

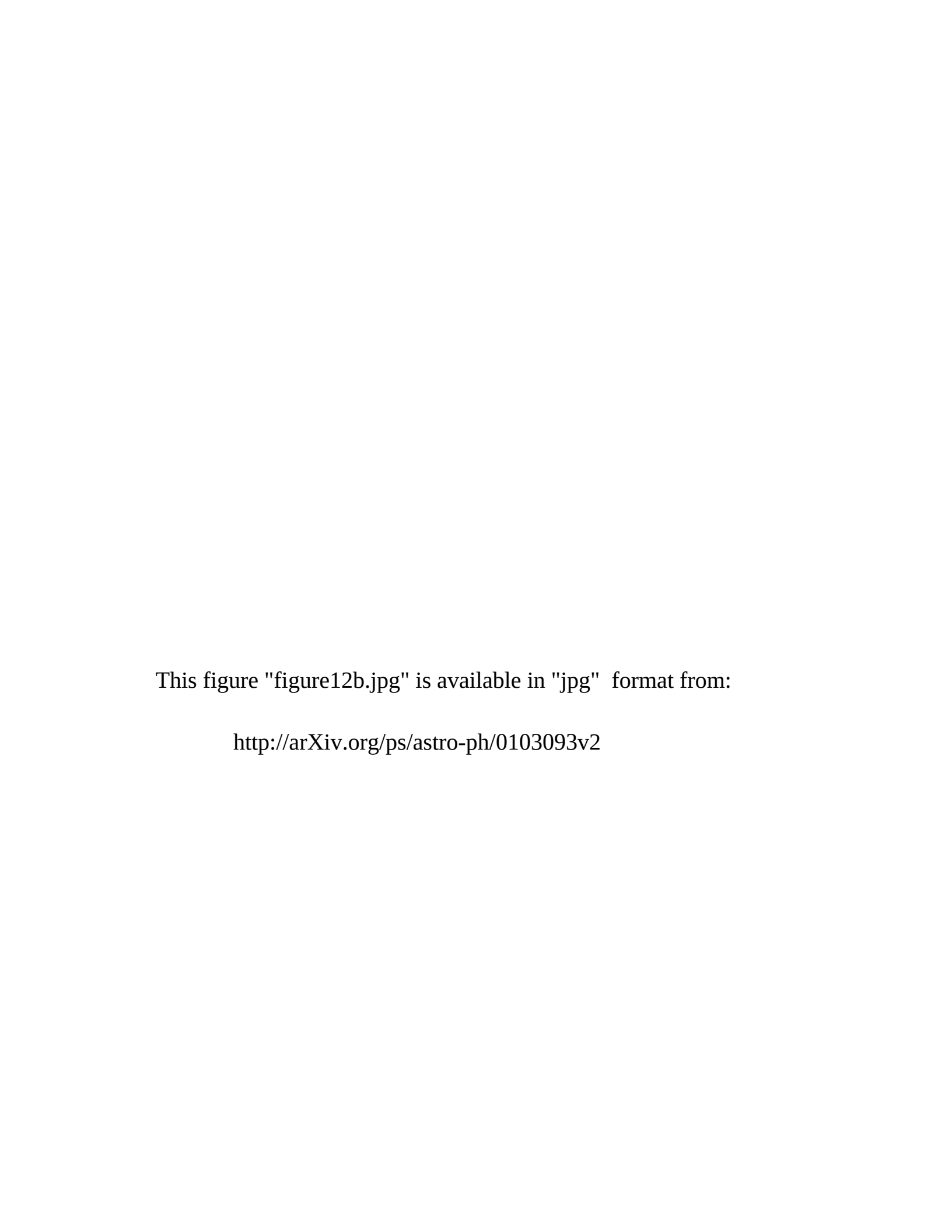
This figure "figure12b.jpg" is available in "jpg" format from:
http://arXiv.org/ps/astro-ph/0103093v2

This figure "figure12c.jpg" is available in "jpg" format from:

http://arXiv.org/ps/astro-ph/0103093v2

This figure "figure12d.jpg" is available in "jpg" format from:

http://arXiv.org/ps/astro-ph/0103093v2